Comparison of the Huggins Band for Six Ozone Isotopologues: Vibrational Levels and Absorption Cross Section

ARTICLE *in* THE JOURNAL OF PHYSICAL CHEMISTRY A · SEPTEMBER 2012

Impact Factor: 2.69 · DOI: 10.1021/jp3064382 · Source: PubMed

THE JOURNAL OF PHYSICAL CHEMISTRY A

Article

pubs.acs.org/JPCA

Comparison of the Huggins Band for Six Ozone Isotopologues: Vibrational Levels and Absorption Cross Section

Steve Alexandre Ndengué

Université de Grenoble 1/CNRS, LIPhy UMR 5588, Grenoble, F-38041, France Laboratoire de Physique Fondamentale, Université de Douala, BP 2071 Douala, Cameroun

Reinhard Schinke

Max Planck Institut für Dynamik und Selbstorganisation, D-37073 Göttingen, Germany

Fabien Gatti

CTMM, Institut Charles Gerhardt, UMR 5253, CC 1501, Université de Montpellier II, F-34095 Montpellier, Cedex 05, France

Hans-Dieter Meyer

Theoretische Chemie, Physikalisch-Chemisches Institut, Im Neuenheimer Feld 229, Universität Heidelberg, 69120 Heidelberg, Germany

Rémy Jost*

Université de Grenoble 1/CNRS, LIPhy UMR 5588, Grenoble, F-38041, France

Supporting Information

ABSTRACT: By use of the $3^1A'$ ab initio potential energy surface (PES) of ozone and the multi-configuration time-dependent Hartree program for wavepacket propagation, we have determined numerous eigenstates of this state for six ozone isotopologues. These bound vibrational levels are the upper levels of the Huggins band, which covers the range from 27 000 to ~33 000 cm^{-1}. This study extends our previous work on the Hartley band, which was limited to the range ~32 000−50 000 cm^{-1}. Four isotopologues, $^{16}O_3$, $^{16}O^{17}O^{16}O$, $^{16}O^{18}O^{16}O$, and $^{18}O_3$ (noted hereafter 666, 676, 686, and 888), are symmetric, and two are asymmetric, $^{17}O^{16}O_2$ and $^{18}O^{16}O_2$ (noted hereafter 667 and 668). The PES of the $3^1A'$ state has two equivalent minima of C_s symmetry located at ~27 000 cm^{-1} above the X^1A_1 ground state. The equilibrium geometry of these two minima is r_{e_1} = 2.28 a_0, r_{e_2} = 3.2 a_0, and θ_e = 107°. The dissociation limit of this PES, which correlates to the $O(^1D) + O_2(^1\Delta)$ "singlet" channel, is about 4300 cm^{-1} above the two minima. For the $^{16}O_3$ isotopologue, the 120 lowest bound eigenstates have been calculated and partially assigned up to 800 cm^{-1} below the dissociation limit. The 60 lower eigenstates are easily assignable in term of three normal modes, the "long" bond (ν_1), the bending (ν_2), and the "short" bond (ν_3). A new family of wave functions, aligned along the dissociation channels, appears at 3782 cm^{-1} above the $3^1A'$ (0,0,0) level. The $3^1A'$ vibrational levels and the corresponding intensity factors from the (000), (010), (100), and (001) levels of the X^1A_1 ground state have been calculated for the six isotopologues. The Huggins absorption cross sections of the six isotopologues have been calculated from the $3^1A'$ vibrational energy levels and the corresponding intensity factors. The rotational envelope of each vibronic band has been empirically described by an ad hoc function. The ratio of the Huggins cross section of each ozone isotopologue with one of $^{16}O_3$ provides the fractionation factor of each ozone isotopologue as a function of the photon energy. These various fractionation factors will allow predicting enrichments due to photolysis by various light sources like the actinic flux.

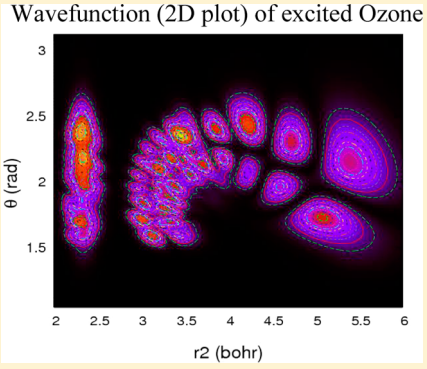

1. INTRODUCTION

In the atmosphere, the ozone molecules are continuously formed and destroyed. The destruction is due to photolysis,

Received: June 29, 2012
Revised: September 24, 2012
Published: September 24, 2012

according to the Chapman process,[1] and to chemical reactions with NO_x, ClO_x, and HO_x. The resulting steady state ozone isotopologue ratios are the net result of the isotopologue selectivities of the formation and destruction processes. The isotope selectivity of the formation process has been first determined experimentally by Thiemens and Heidenreich[2] and the Mauersberger group[3,4] and then interpreted by theoreticians with and ad hoc model.[5,6]

The isotopologue selectivity of the photolysis process, which motivated this study, is poorly known: in 2003 Chakraborty and Bhattacharya[7] found experimentally a "mass-independent" photodissociation process, but Cole and Boering[8] abandoned their interpretation. In 2005 and 2006, Miller et al.[9] and Liang et al.[10] reported a mass-dependent enrichment in the photodissociation process using a semiempirical model[11] to generate the absorption cross sections of rare isotopologues in the visible and UV ranges. Their calculations neglect the contribution of the ∼315−410-nm range which corresponds to the Huggins band and the high energy part of the Chappuis band. This choice is unexpected because the same group has predicted an "extraordinary" isotopic fractionation in the Huggins range.[9]

Experimentally it is very difficult to isolate ozone isotopologues such as $^{18}O^{16}O_2$ or $^{16}O^{18}O^{16}O$ and then to measure their absorption cross sections. In contrast, cross sections of various ozone isotopologues can be obtained (and then compared) using quantum calculations, because these isotopologues have the same potential energy surfaces (PESs) within the Born−Oppenheimer approximation. In a previous paper, hereafter termed Paper I,[12] using the wavepacket propagation multi-configuration time-dependent Hartree (MCTDH) code,[13,14] we have compared the low resolution Huggins−Hartley absorption cross sections of 18 isotopologues in the range of 31 000−50 000 cm^{-1}. Below ∼31 000 cm^{-1}, the absorption cross section computed with the MCTDH wavepacket propagation code is very noisy because of its very weak amplitude (more than 4 orders of magnitude weaker than at the maximum of the Hartley cross section). This limitation should be overcome because the Huggins band plays a significant role in the atmospheric ozone photolysis below ∼30 km. This numerical limitation has been solved by obtaining the absorption cross section of each isotopologue from its $3^1A'$ vibrational energies and the corresponding intensity factors. Experimentally, the band origin of these vibrational levels cannot be determined accurately because of the rotational congestion and of the predissociation due to the R state.[15] The calculated and experimental absorption cross sections can easily be compared only for the $^{16}O_3$ and $^{18}O_3$ isotopologues. The observed differences between the calculated and experimental absorption cross sections are due mainly to the imperfections of the $3^1A'$ PES. This paper is focused on the isotopologue shifts of the $3^1A'$ vibrational energy levels and of the related Huggins absorption cross sections because these shifts are responsible of the isotopologue enrichment due to the photolysis process.

This paper is organized as follows: we present in section 2 the calculations of vibrational levels with the MCTDH code, in section 3 the energies and assignments of the $3^1A'$ vibrational levels of six isotopologues, in section 4 the Huggins absorption cross sections for various ozone isotopologues and the related fractionation factors, and in section 5 the conclusions and perspectives.

2. CALCULATIONS OF VIBRATIONAL LEVELS WITH THE MCTDH CODE

The Huggins band of ozone covers the 27 000−32 000-cm^{-1} energy range of the absorption cross section to the $3^1A'$ state, while the Hartley band corresponds to the 32 000−50 000-cm^{-1} range of the same electronic transition. The 32 000-cm^{-1} frontier is chosen for convenience and has no real meaning. 2D contour plots of the $3^1A'$ PES along the r_1,r_2 and θ,r_1 internal coordinates are shown in Figure 1.

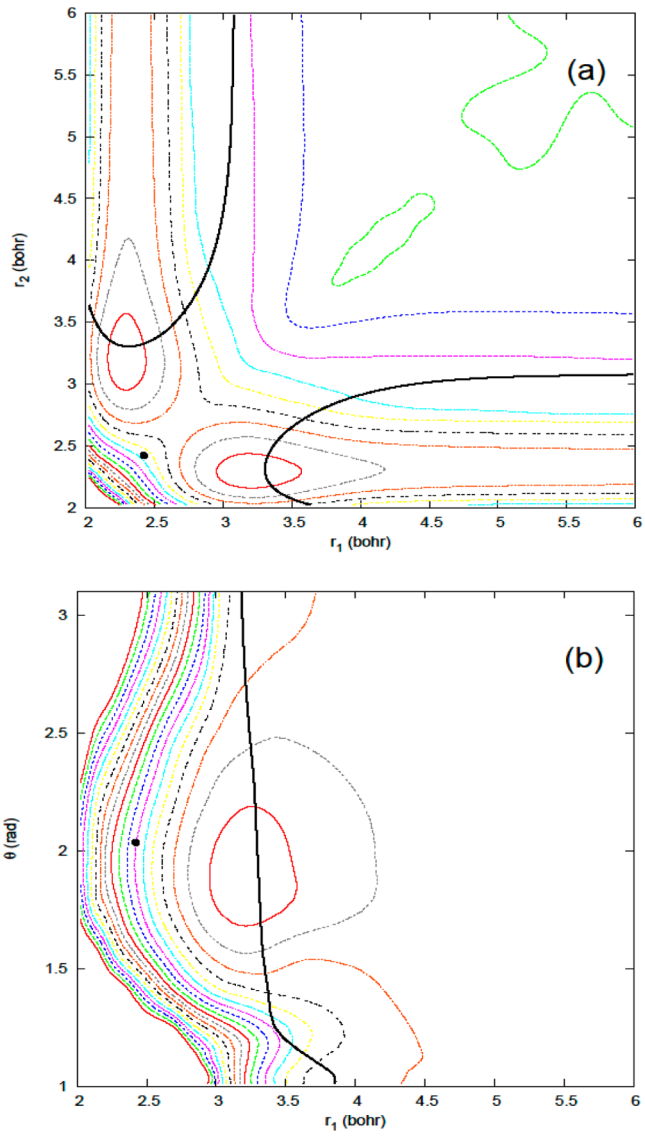

Figure 1. 2D contour plot of the $3^1A'$ PES. (a) r_1,r_2 representation with θ =116.6°. (b) r_1,θ representation with r_2 = 2.422 a_0. The dot locates the minimum of the ground-state PES (r_1 = r_2 = 2.423 a_0, θ =117°). The spacing between the lines is 0.5 eV (4033 cm^{-1}). The black lines are the intersections of the R state with the $3^1A'$ state.

The $3^1A'$ PES, which was computed by R. Schinke and McBane,[15] has two equivalent shallow minima of C_s symmetry. Their equilibrium geometries are located, respectively, at r_1 = 3.21 a_0, r_2 = 2.28 a_0, θ = 1.87 rad and r_2 = 3.21 a_0, r_1 = 2.28 a_0, θ = 1.87 rad.

The bound vibrational eigenstates are computed with the MCTDH package. MCTDH[14,16,17] is a method in which each

dx.doi.org/10.1021/jp3064382 | J. Phys. Chem. A 2012, 116, 12260−12270

degree of freedom is associated with a small number of orbitals or single-particle functions (SPFs) which, through their time dependence, allow efficient description of the entire molecular dynamics process. The total wave function is expanded in Hartree products, that is, products of single-particle functions.

$$\Psi(Q_1,\ldots,Q_f,t) = \sum_{j_1=1}^{n_1}\cdots\sum_{j_f=1}^{n_f} A_{j_1\cdots j_f}(t)\prod_{\kappa=1}^{f}\phi_{j_\kappa}^{(\kappa)}(Q_\kappa,t) \quad (1)$$

Here, f is the number of degrees of freedom of the system, Q_1, ..., Q_f are the nuclear coordinates, $A_{j1\cdots jf}$ denote the MCTDH expansion coefficients, and $\varphi_{j\kappa}(\kappa)(Q_\kappa, t)$ are the n_k SPFs associated with each degree of freedom κ. To solve the equations of motion the SPFs are represented on a primitive basis or discrete variable representation (DVR) grid. Thus, the MCTDH method propagates a wave function on a small time-dependent, variationally optimized basis set of single-particle functions, which in turn are defined on a time-independent primitive basis set with N_κ points for the κth degree of freedom.

The block-improved relaxation method, a variant of the improved relaxation method,[18,19] implemented in the MCTDH package is used for our computations. The improved relaxation method is a MCSCF approach where the SPFs are optimized by relaxation[20] (propagation in negative imaginary time) but the coefficients vector (A-vector) is determined by diagonalization of the Hamiltonian matrix evaluated in the set of the present SPFs. The block form of improved relaxation is an efficient way of computing several eigenstates simultaneously. A block of initial vectors are propagated to converge collectively to a set of eigenstates. At lower energies, a block of 10 eigenstates packets were selected to obtain the desired eigenstates. At about 3500 cm^{-1} above (0,0,0), computations were made with a block of 4 eigenstates packets as convergence turned out to be more difficult to achieve with a larger block. Also, while 20 SPFs along r_1, r_2, and θ are sufficient to converge at low energies, 40, 40, and 30 SPFs along r_1, r_2, and θ, respectively, are needed to converge our computations close to the dissociation limit. A sine DVR representation between 1.8 and 12.0 a_0 along the valence bond and a restricted Legendre DVR representation between 1.05 and 3.067 rad along the valence angle were used for our computations. The constant mean field (CMF) integration scheme was used with the Davidson routine applied for the diagonalization of the A-vector and Runge−Kutta of order 8 for the integration of SPFs. The parameters for the computations of the vibrational eigenstates are recorded in Table 1.

The vibrational energy levels and the corresponding wave functions are described in the next section. The wave functions are used to visually assign the normal mode quantum numbers and to calculate the relative intensities of the various vibronic bands with the integral

$$I_{ij} = |\langle\psi_i(r_1,r_2,\theta)|\mu(r_1,r_2,\theta)|\phi_j(r_1,r_2,\theta)\rangle|^2 \quad (2)$$

where ψ_i and φ_j are the initial and final vibrational wave functions (here, respectively, those of the ground-state X^1A_1 and $3^1A'$ PESs) and $\mu(r_1,r_2,\theta)$ is the transition dipole moment surface (TDMS). This expression is a generalization of the Franck−Condon factor which includes the TDMS. For a given electronic transition, i and j correspond to the vibrational assignments of the initial and final levels.

Table 1. Parameters for the Computation of the Huggins Band Vibrational Levels[a]

	r_1	r_2	θ
primitive basis	sine DVR	sine DVR	Leg/R DVR
N	256	256	128
grid	[1.8, 12.0]	[1.8, 12.0]	[1.05, 3.067]
n	20−40	20−40	20−30
	r_1	r_2	θ
integrator	scheme	A-vector	SPF
type	CMF	rDAV	RK8
initial time interval/max. order	1.0		900
accuracy	10^{-3}	10^{-9}	10^{-8}

[a] N is the number of functions in the primitive basis, and n is the number of SPFs. Leg/R is the restricted Legendre DVR. CMF is the constant mean field integration scheme. RK8 is for Runge−Kutta of order 8, and rDAV is the Davidson integrator for a real Hamiltonian. More details are given in the text.

3. $3^1A'$ EIGENSTATES OF SIX OZONE ISOTOPOLOGUES

3.1. $^{16}O_3$ $3^1A'$ Vibrational Eigenstates. We present the analysis of the calculated $3^1A'$ vibrational eigenstates for the $^{16}O_3$ (or 666) isotopologue. The analyses for the other isotopologues are very similar and not detailed below. However, the two asymmetric isotopologues, 667 ($^{16}O_2{}^{17}O$) and 668 ($^{16}O_2{}^{18}O$), require additional information presented in section 3.2. The vibrational energies and vibrational assignments are available as Supporting Information.[21] By use of the notation of Grebenshchikov et al.,[22] the three normal modes of the $3^1A'$ state are the "long bond", (indexed with the ν_1 quantum number), which corresponds mostly to an excitation of the longest bond (around r_e =3.2 a_0), the bending mode (ν_2), and the "short bond" (ν_3), which corresponds mostly to an excitation of the shortest bond (around r_e =2.28 a_0). The eigenstates have also been classified in term of polyad number because the three normal-mode frequencies are approximately in the ratio 2:1:4. Each polyad is made of the vibrational levels having the same $P = 2\nu_1 + \nu_2 + 4\nu_3$. The number of levels per polyad increases from 1 level for P = 0 and 1 to 12 levels for P = 10 and 11. The vibrational and polyad assignments start to fail at $P \approx 10$, in part because of the overlapping of adjacent polyads which allows interpolyad couplings. The assignments are secure for all the levels up to number 50, at 3337 cm^{-1}. In some cases, at higher energies, only ν_3, the short bond, can be determined, ν_1 and ν_2 being not well-defined. In that case, the eigenstate is assigned as (?,?,ν_3). When the assignment seems impossible or doubtful we use the (?,?,?) notation.

The wave function of each vibrational level listed in Table 2[21] has been represented by three 2D plots in the $\{\theta,r_1\}$, $\{\theta,r_2\}$ and $\{r_1,r_2\}$ planes. The assignments of the energy levels have been done mostly by visual inspection of these plots using three quantum numbers. The criterion for assignment is the number of nodal lines along each of the three curved classical trajectories that are associated to the three normal mode directions. The assignments are straightforward at low energies and more and more difficult and ambiguous with increasing energy. The assignments are made easier owing to the predictions of a Dunham expansion, the new assignments allowing iterative improvement of the set of Dunham parameters. For example, the wave function contour plots in

Table 2. 26 Lowest Vibrational Levels of the Symmetric 666, 676, 686, and 888 Isotopologues[a]

	isotopologue energies (cm^{-1})			
(ν_1,ν_2,ν_3)	666	676	686	888
(0,0,0)	0	0	0	0
(0,1,0)	375.062	373.438	371.875	354.683
(1,0,0)	680.824	669.65	659.6	643.571
(0,2,0)	736.406	733.203	730.16	696.771
(1,1,0)	1052.606	1040.407	1029.28	995.704
(0,3,0)	1089.592	1084.89	1080.453	1031.12
(2,0,0)	1325.946	1304.133	1284.513	1255.021
(1,2,0)	1402.082	1394.11	1381.06	1333.534
(0,0,1)	1409.779	1383.745	1366.035	1325.968
(0,4,0)	1437.867	1431.941	1426.312	1360.853
(2,1,0)	1691.907	1670.024	1650.205	1602.747
(1,3,0)	1743.644	1728.606	1714.661	1652.83
(0,1,1)	1776.814	1756.62	1737.278	1679.339
(0,5,0)	1784.305	1775.538	1768.542	1688.45
(3,0,0)	1944.251	1912.124	1883.19	1842.586
(2,2,0)	2034.899	2012.068	1991.299	1930.308
(1,4,0)	2071.167	2054.644	2043.447	1964.524
(1,0,1)	2092.407	2062.32	2031.157	1978.308
(0,6,0)	2120.209	2109.34	2105.867	2007.919
(0,2,1)	2137.859	2116.864	2091.13	2020.919
(3,1,0)	2295.537	2264.385	2236.284	2178.802
(2,3,0)	2356.246	2333.427	2312.469	2239.118
(1,5,0)	2395.067	2379.14	2364.327	2273.135
(1,1,1)	2449.353	2418.494	2389.35	2317.79
(0,7,0)	2453.679	2442.225	2431.791	2325.205
(0,3,1)	2485.534	2460.934	2439.764	2350.191

[a]The first column is the identification with the normal modes of vibration, long bond, bending, and short bond, respectively, for ν_1, ν_2, and ν_3. The four other columns are the two-fold degenerated vibrational energies with the (0,0,0) of each isotopologue taken as a reference.

the θ,r_2 plane of the (2,3,0) and (2,0,1) levels are shown in Figure 2.

These two wave functions, of number 22 (at 2356 cm^{-1}) and number 31 (at 2738 cm^{-1}), can easily be assigned by counting their nodal lines (see the caption of Figure 2). At 3782 cm^{-1} the first member of a new family of wave functions appears (level number 71): the wave functions of this family cannot be assigned in continuity with the lower eigenstates. These new type of eigenstates have no excitation in the short bond (they have ν_3 = 0), but they cannot be interpreted in terms of the long bond (ν_1) and the bending (ν_2) vibration. Instead, their wave functions are elongated along a new type of periodic orbit elongated toward the O_2 + O dissociation channel, the short bond corresponding, for large long bond distance, to the O_2 vibrational mode. The family is labeled as (hs *i*,*j*) where "hs" stands for "horseshoe", "*i*" identifies the number of the function, and "*j*" the quantum number along the short bond (as for the other assignments). This family starts around 3782 cm^{-1} but ends quite quickly at 4169 cm^{-1}. Two examples of this family are shown in Figure 3.

Other types of wave functions are also observed, but they do not persist at higher energies.

3.2. Comparison of the $3^1A'$ Vibrational Eigenstates of Six Isotopologues. The 26 lower $3^1A'$ vibrational energy levels of the four symmetric and the two asymmetric isotopologues are listed in Tables 2 and 3.

The full lists of the vibrational energy levels of the 6 isotopologues are available in Tables 4−9 of the Supporting Information[21] in which the vibrational levels have been numbered (first column) by increasing energy (second column) and some have been assigned (third column), mostly with the three normal modes, (ν_1,ν_2,ν_3). The polyad numbers are given in the fourth column. The intensity factors from the 4 lowest X^1A_1 vibrational levels, (0,0,0), (0,1,0), (1,0,0), and (0,0,1), (columns five to eight) have been normalized to the value of the (0,0,0) → (0,0,0) transition of each ozone isotopologue or isotopomer. These intensity factors allow including the weighted contributions of the cold and hot bands to the absorption cross section (see section 4) at various temperatures.

To visualize the similarities and the differences between the polyad structures of the various isotopologues, the 14 lower-energy levels of four isotopologues are compared in Figure 4.

The pair of vibrational levels of the 8—6—6 and 6—6—8 isomers having the same assignment are shifted in energy. So, a

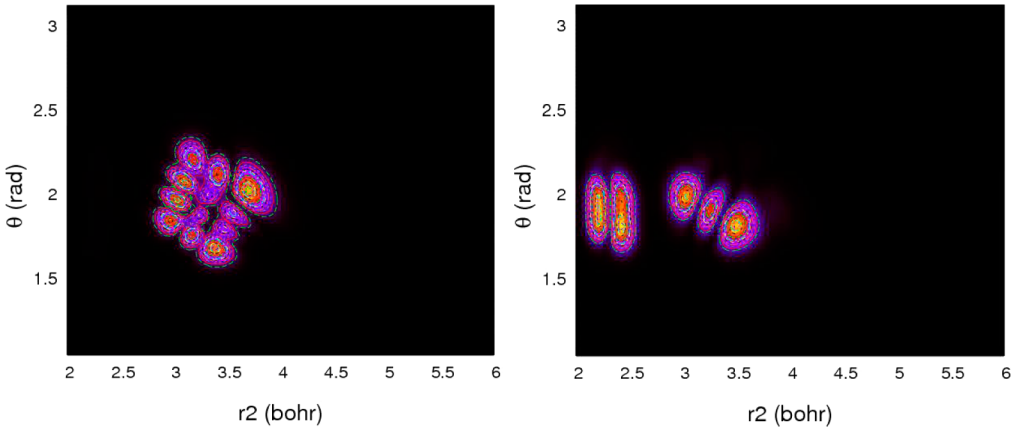

Figure 2. 2D contour plots of the (2,3,0) (left) and the (2,0,1) (right) wave functions in the θ,r_2 plane. On the left plot, the r_2 coordinate is the longest bond, and the shortest bond is not represented (the wave function has no nodal line along the shortest bond). The nodal lines are not aligned, respectively, with the θ and the r_2 coordinates but are perpendicular to the bending (3 nodal lines) and the long bond (2 nodal lines) normal coordinates. On the right plot, the r_2 coordinate represents the short bond between 2 and 2.75 a_0, showing one nodal line (almost perpendicular to the short bond), and represents the long bond above.

dx.doi.org/10.1021/jp3064382 | J. Phys. Chem. A 2012, 116, 12260−12270

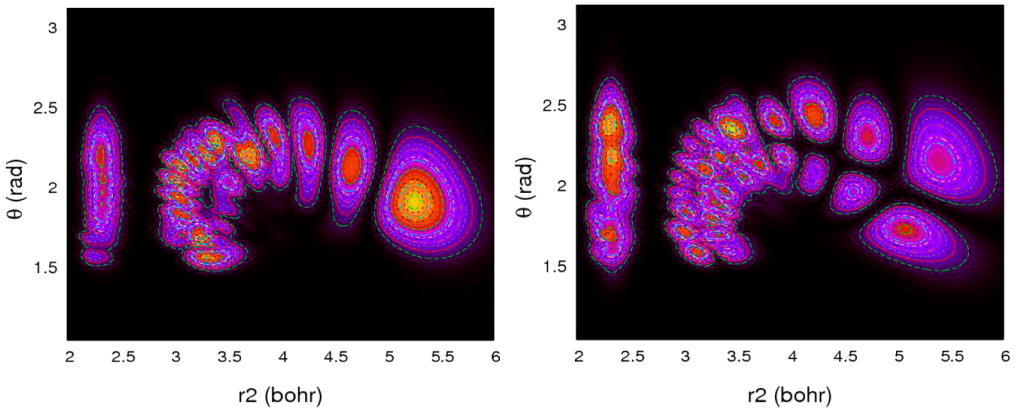

Figure 3. 2D contour plots of two "horseshoe" wave functions of the Huggins band. They are numbered 95 (left) and 100 (right). r_2 is a dissociation coordinate corresponding to the O_2 + O channel. As for the right plot of Figure 2, the r_2 coordinate correspond to the short bond between 2 to 2.75 a_0 (showing no nodal line (ν_3 = 0) and to the long bond above 2.75 a_0 showing a complex nodal structure, named "horseshoe" in the text, and elongated toward the O + O_2 dissociation channel.

Table 3. 26 Lowest Vibrational Levels of the Asymmetric 667 and 668 Isotopologues[a]

	isotopologue energies (cm^{-1})			
(ν_1,ν_2,ν_3)	6--67	66--7	6--68	66--8
(0,0,0)	0	6.707	0	12.732
(0,1,0)	370.442	377.309	366.242	379.227
(1,0,0)	680.144	680.092	679.477	679.504
(0,2,0)	727.517	734.445	719.493	732.496
(1,1,0)	1047.371	1047.062	1042.39	1042.02
(0,3,0)	1076.522	1083.532	1064.858	1077.821
(2,0,0)	1324.391	1319.377	1322.901	1313.61
(1,2,0)	1398.753	1395.782	1389.614	1387.441
(0,0,1)	1384.753	1412.927	1367.597	1415.717
(0,4,0)	1420.32	1427.915	1404.547	1421.179
(2,1,0)	1686.044	1680.102	1680.48	1669.469
(1,3,0)	1729.707	1731.384	1715.888	1719.808
(0,5,0)	1761.859	1766.463	1741.675	1782.665
(0,1,1)	1754.652	1781.654	1735.848	1753.558
(3,0,0)	1941.707	1933.244	1939.405	1923.527
(2,2,0)	2025.187	2019.775	2015.97	2005.877
(1,4,0)	2053.397	2055.346	2037.003	2040.587
(1,0,1)	2072.77	2090.926	2055.218	2085.023
(0,6,0)	2095.27	2102.241	2072.827	2090.254
(0,2,1)	2110.016	2134.862	2085.263	2132.324
(3,1,0)	2289.387	2279.384	2283.698	2264.889
(2,3,0)	2342.368	2338.63	2329.06	2322.416
(1,5,0)	2374.244	2375.11	2355.478	2356.686
(1,1,1)	2428.767	2445.615	2407.347	2440.239
(0,7,0)	2422.767	2429.634	2397.762	2409.442
(0,3,1)	2453.308	2478.823	2424.454	2472.686

[a]The first column is the identification with the normal modes of vibration, long bond, bending, and short bond, respectively, for ν_1, ν_2, and ν_3. For each isotopologue, the progression along each of the C_s wells is written, for example, as 6--68 and 66--8 to identify the potential well (see text). The lowest (0,0,0) vibrational energy of each isotopologue is taken as reference for the progression along each of the wells.

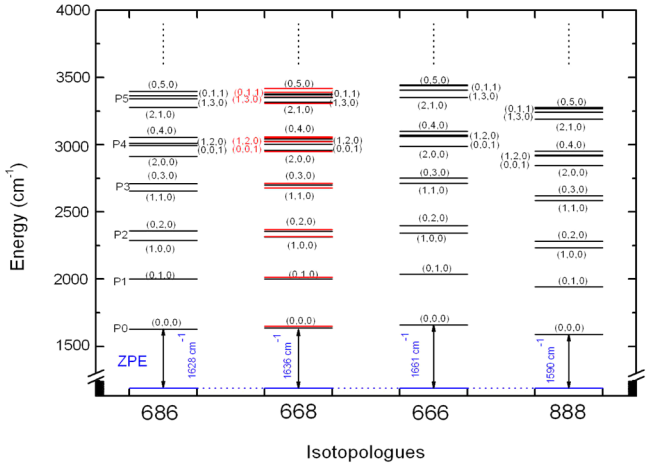

Figure 4. Comparison of the 14 lower $3^1A'$ vibrational energies of four ozone isotopologues 686, 668, 666, and 888. The six lowest polyads (P = 0–5) are shown. The energies are given in Tables 2 and 3 of the text and Tables 4–7 of the Supporting Information for the various isotopologues. The vibrational levels for the symmetric isotopologue are doubly degenerate. In contrast, the 668 asymmetric isotopologue has two progressions corresponding to the 6–68 (in black) and 66–8 (in red) isomers. The zero-point energy of 1636 cm^{-1} is for the 6–68 isotopomer. The zero-point energy of 66–8 is 1649 cm^{-1}.

symbol, like 8—6–6 or 6—6–8 should be used in addition to (ν_1,ν_2,ν_3) to distinguish the levels of the two isomers. It should be noted that the dissociation limits of these two families differ by 22.1 cm^{-1}, which is the difference between the zero-point energy (ZPE) of the $^{16}O_2$ and the $^{18}O^{16}O$ dissociation products. Note that the intensity factors (of the transitions starting from the X^1A_1 (0,0,0), (1,0,0), (0,1,0), and (0,0,1) ground-state levels) have been normalized to the intensity factor for the (0,0,0) level of each isomer (which is equal to 1 by definition). These two Franck–Condon factors corresponding to the (0,0,0) level of each isomer are significantly different, with a ratio of (0.56/0.44) = 1.27 in favor of the 6—6–8. The specific cases of the 668 and 667 asymmetric isotopologues are important in terms of atomic oxygen enrichment due to ozone photodissociation and will be analyzed elsewhere.[23]

In 2004, Qu et al.[24] have calculated the $3^1A'$ vibrational levels of $^{16}O_3$ with a PES which differs slightly from the one used in this paper. The comparison of their vibrational energies and assignments shows systematic trends. First, their vibrational energies are higher than the ones given in Table 2. For example, the three fundamental frequencies are higher by 3.2, 3.2, and 6% than the ones of Table 2. The comparison of the calculated and experimental cross sections (see below) shows that our

dx.doi.org/10.1021/jp3064382 | J. Phys. Chem. A 2012, 116, 12260–12270

vibrational energies given in Table 2 are significantly closer to the experimental energies than those of Qu et al.[24]

Second, the order (ranking) of their vibrational assignments differ from the one given in Table 2. There are many permutations, the first one occurring for the levels (4,0,0) and (0,3,1) of number 26 and 27 around ∼2500 cm^{-1}. Third, and more surprising, Qu et al. give all the assignments up to the level ranked 89 (at 4263 cm^{-1}), while we have not been able to assign most of the levels above the level number 76 (at 3860 cm^{-1}). These differences indicate that the mode coupling associated to the PES used in this paper is stronger than the coupling caused by the PES used by Qu et al. This is confirmed by the appearance, at 3782 cm^{-1}, of a new type of wave functions (see above) corresponding to a new classical periodic orbit. In contrast, Qu et al.[24] have assigned all the wave functions up to 4265 cm^{-1} with three normal mode quantum numbers. In 2006 Farantos et al.[25] obtained one wave function similar to the "horseshoe" mentioned above and linked it to the bifurcation in their nonlinear dynamics analysis. Such "horseshoe" wave functions have been observed for the six studied isotopologues.

An accurate comparison of the calculated and experimental Huggins vibrational energies is not easy because the experimental eigenstates are predissociated and then not well resolved. The vibrational assignments proposed by Katayama[26] have been obtained owing to the comparison of the $^{16}O_3$ and $^{18}O_3$ absorption spectra. These assignments have been revised two times,[27,28] the ones of O'Keeffe et al.[28] being in reasonable agreement with those of Qu et al.[24] and with those given in Table 2 both being derived from ab initio PESs, even if some ambiguous assignments remain at high energies as discussed above. Below, in section 4.3, we make only a comparison of the $^{16}O_3$ calculated and experimental low resolution cross sections in the Huggins range.

4. THE HUGGINS ABSORPTION CROSS SECTION OF SIX OZONE ISOTOPOLOGUES

4.1. Cross Sections Obtained with a Wavepacket Propagation. In our previous paper I[12] the absorption cross section of each isotopologue, has been determined, in the range of the Hartley band, with the MCTDH code from a propagation of $\Psi(0)$, the ground-state (0,0,0) wave function, on the PES of the $3^1A'$ electronic state. The absorption cross section of ozone in the Hartley/Huggins band was obtained from the Fourier transform of the autocorrelation function

$$\sigma(\omega) \propto \int_{-\infty}^{+\infty} \langle \Psi(0)|\Psi(t)\rangle \, dt = \int_{-\infty}^{+\infty} \langle \Psi(0)|e^{-i\hat{H}t/\hbar}|\Psi(0)\rangle \, dt \quad (3)$$

The various cross sections presented below, named "propagation" cross sections, and obtained with this time dependent method are numerically accurate at least down to 31 000 cm^{-1}. Meanwhile, this set of "propagation" cross section, shown in black in Figure 5 for the 666 isotopologue, is noisier with decreasing energy, especially below ∼31 000 cm^{-1}. This numerical noise is induced by the very large amplitude of the Hartley band around 40 000 cm^{-1} where the "propagation" cross section is 4−6 orders of magnitude stronger than between 30 000 and 27 000 cm^{-1}. The "propagation" cross section can be artificially improved by smoothing. This smoothing has the advantage of decreasing the numerical noise but the disadvantage of reducing the spectral resolution. Here, the critical resolution is of the order of the polyad interval (∼300 cm^{-1}) which is clearly seen both on the experimental and calculated cross sections. Such a smoothing, which has been used in paper I, allows a satisfactory cross section to be obtained with the MCTDH propagation method (see above) down to ∼29 000 cm^{-1}. This is why, in Figures 8 and 9 of paper I,[12] the Huggins part of the "propagation" cross sections is not shown below 29 000 cm^{-1}, a range corresponding to polyads $P < 6$.[29] The noisy part of the "propagation" cross section can be replaced by the cross section obtained by the Franck-Condon (FC) method presented in the next section. An example is shown in Figure 5, where the numerical noise is present at energies below ∼31 500 cm^{-1}.

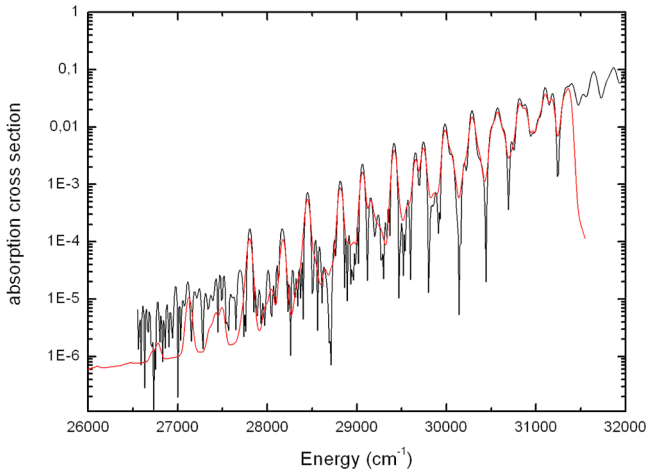

Figure 5. Comparison of the 666 absorption cross sections calculated with the FC method (in red) and with the propagation method (black, noisy). The polyad $P = 0$ corresponds to the red peak at 27 112 cm^{-1}. The best overall cross section is made of the F.C. cross section below 31 200 cm^{-1} and the propagation cross section above 31 200 cm^{-1}. The propagation cross section has been obtained after a propagation of 70 fs. The amplitude of the vibronic structures depends on the propagation duration and then has no reason to match the amplitude of the vibronic structures of the FC cross section which has been chosen to mimic the experimental rotational envelope. However, the averaged amplitudes of the propagation cross section and of the FC cross section should coincide. It is why the amplitude of the FC cross section has been normalized in order to have the same average amplitude as the propagation cross section between 29 000 and 31 200 cm^{-1}. A global shift of −450 cm^{-1} (toward low energies) has been applied to both cross sections (see section 4.4).

4.2. Huggins Cross Sections Obtained with the FC Method. This method uses the bound vibrational energies of the $3^1A'$ and the corresponding intensity factors. Below the cross sections obtained with this method are named FC cross sections. In a first step, this FC method provides a stick cross section made of sticks at the bound vibrational energies with amplitude proportional to their intensity factors. These energies and intensity factors are listed in Tables 4−9 of the Supporting Information. These stick FC cross sections have been convoluted with an ad hoc Θ function, which is the result from a convolution of a Lorentzian and a modified Gaussian function

$$\Theta_{C,L_G,A,L_L}(E) = G_{C,L_G,A}(E) \times L_{C,L_L}(E) \quad (4)$$

where

dx.doi.org/10.1021/jp3064382 | J. Phys. Chem. A 2012, 116, 12260−12270

$$G_{C,L_G,A}(E) = \begin{cases} \exp\left[-\left(\frac{E-C}{L_G - A}\right)^2\right] & \text{if } E \geq C \\ \exp\left[-\left(\frac{E-C}{L_G + A}\right)^2\right] & \text{if } E \leq C \end{cases} \quad (5)$$

and

$$L_{C,L_L}(E) = \frac{1}{1 + \left(E - \frac{C}{L_L}\right)^2} \quad (6)$$

This empirical Θ function mimics both the rotational envelope and the predissociation widths due to the R state which was not included in our MCTDH relaxation calculations.

In eqs 4−6, E is the energy, the continuous variable which describes the cross section, C the energy of each vibrational level, L_G the Gaussian width, A the asymmetry of this Gaussian, and L_L the Lorentzian width characterizing the predissociation line width. The predissociation lifetime of the levels corresponding to the Huggins band has been estimated to be in the range of 1−4 ps.[15] The asymmetry parameter A allows to mimic the asymmetry due to the rotational envelope of each experimental vibronic bands (Figure 6). A single set of

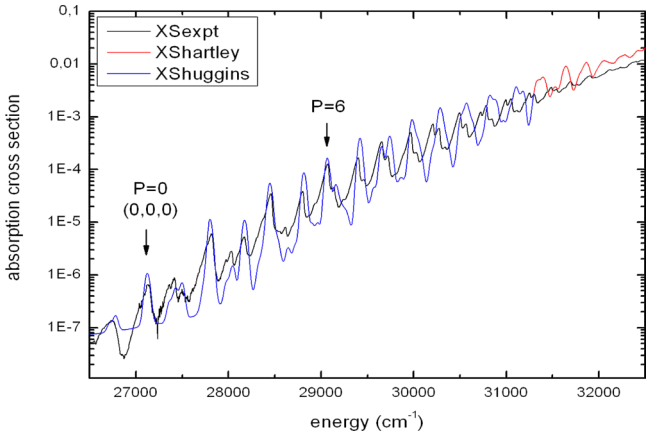

Figure 6. Comparison of the calculated and experimental $^{16}O_3$ (or 666) absorption cross sections in the Huggins range. The experimental cross section (218 K) is in black, and the calculated cross section (200 K) is in blue below 31 250 cm^{-1} and in red above. The blue and red parts have been obtained, respectively, with the FC and the propagation methods. The "calculated" cross section is shifted by 450 cm^{-1} to low energies (see text). The shifts between the experimental and calculated polyad energies which increase progressively with energy are discussed in the text.

parameters, L_G = 35 cm^{-1}, L_L = 5 cm^{-1}, and A = 15 cm^{-1}, has been used to describe the shape of all the vibrational bands included in the calculated FC cross section in the range of the Huggins band. This set of three parameters has been chosen in order to get a rough visual agreement (Figure 6) between the experimental Huggins cross section of $^{16}O_3$ at 218 K and the one calculated with our FC method. The same set of three parameters has been used for the six isotopologues because we do not expect a significant change of the predissociation lifetime nor of the shape of the rotational envelop. The calculated vibrational energy of the $3^1A'(0,0,0)$ level is 27 562 cm^{-1} from the $X^1A_1(0,0,0)$ level. The maximum of the corresponding envelope obtained from eqs 4−6 is at 27 577 cm^{-1}. The shift of 15 cm^{-1} between these two values mimics the experimental shift between the band origin and the maximum of the rotational envelope. This shift will be neglected.

4.3. Comparison of the $^{16}O_3$ Experimental and Calculated Huggins Cross Sections. In this section we first compare the propagation and the FC cross sections of the $^{16}O_3$ isotopologue and then concatenate these two cross sections into a single calculated cross section and then compare this calculated cross section with the experimental cross section.

By use of the data in Table 4 of Supporting Information,[21] this FC method allows determining the shape of the low-resolution Huggins cross section of the $^{16}O_3$ isotopologue up to about 31 300 cm^{-1} (Figure 5). Our intensity factors combined with our ad hoc Θ function (eq 4), when properly normalized, provide the correct overall amplitude of the cross section. This same overall amplitude is obtained in the propagation method when the transition dipole moment surface (TDMS) is included in the calculation. Figure 5 shows the FC (in red) and "propagation" cross sections (in black) between 26 000 and 32 000 cm^{-1} for the 666 isotopologue. The energy range from ∼27 000 to ∼31 200 cm^{-1} corresponds to the polyads, P = 0 to P = 13, of the Huggins band.

The FC and propagation cross sections displayed in Figure 5 are calculated at 200 K. They are obtained by considering the contributions of the hot bands starting from the four lowest vibrational levels of the ground-state PES. These hot band contributions require (at least) the intensity factors from the four lowest vibrational levels of the ground electronic states, (0,0,0), (0,1,0), (1,0,0), and (0,0,1). The calculated cross section is obtained from the concatenation of the FC cross section from 26 000 cm^{-1} to 31 200 cm^{-1} with the propagation cross section above 31 200 cm^{-1}. However, the $3^1A'(0,0,0) \leftarrow X^1A_1(000)$ calculated energy of 27 562 cm^{-1} is ∼450 cm^{-1} higher than the experimental peak of the $3^1A'(0,0,0) \leftarrow X^1A_1(000)$ band at ∼27 112 cm^{-1}.[28] Consequently, an energy shift of −450 cm^{-1} (to lower energies) has been applied to our FC, propagation, and calculated cross sections (in Figures 5 and 6) in order to get a superposition of the calculated and the experimental $3^1A'(0,0,0) \leftarrow X^1A_1(000)$ vibronic band. This shift is due to an imperfection of the ab initio vertical energy difference between the $3^1A'$ and the X^1A_1 PESs.

A comparison of this calculated cross section of $^{16}O_3$ with the experimental cross section of Brion[30] at 218 K is shown in Figure 6 in the 27 000−31 000-cm^{-1} energy range. The propagation cross section obtained from the Fourier transform of the autocorrelation function was rescaled empirically by a factor of 285/234 to exhibit the same amplitude as the experimental cross section. This rescaling factor is interpreted as a defect of the ab initio TDMS between the X^1A_1 and $3^1A'$ states. These two corrections, the energy shift of −450 cm^{-1} and the amplitude rescaling factor of 285/234, allow getting the reasonable agreement between the calculated and the experimental cross sections displayed in Figure 6.

However, we notice that the average energy spacing between adjacent polyads of the calculated global cross section is slightly larger than the experimental spacing. The polyad energy spacing is controlled by the $(\nu_1,0,0)$ "long" bond progression which has the largest FC factors. This means that the ab initio force constant of the $3^1A'$ along the "long" bond mode is slightly too large compared with the experimental value. The agreement between our calculated and experimental cross

sections is slightly better than the one obtained previously by Qu et al.[24] because the $3^1A'$ PES used here has been slightly improved compared to the one used in 2004 by Qu et al.[24]

4.4. Huggins Cross Section of the Various Isotopologues. With our method of calculation being validated, we have calculated with the same method the Huggins absorption cross section of three symmetric, 686, 676, and 888, and two asymmetric, 866 and 766, isotopologues in order to characterize the effects of the various isotopic substitutions. These various Huggins cross sections have a similar polyad pattern but with significant differences in their polyad energy spacing and their relative amplitudes. For each isotopologue, the polyad pattern is governed by the "long" bond normal mode progression, $(\nu_1,0,0)$, which is almost degenerate with $(\nu_1-1,2,0)$ progression, both progressions having large intensity factors (see Tables 4−9 of the Supporting Information). The $(\nu_1,1,0)$ progression, inserted midway between the peaks of the previous progressions, also has large intensity factors. It is why the apparent polyad spacing is close to half the "long" bond frequency. The polyads are slightly broader for the 686 and 866 isotopologues than for the 666. This explain why the polyad structure is less marked (at a fixed temperature) for these two isotopologues. The smoothed cross sections are significantly weaker in the Huggins range for the heavy isotopologues than for 666. This can be understood in two ways: (a) According to the reflection method,[31] the width of any cross section decreases for an increasing mass. Consequently, the Huggins band, which is nothing else than the low-energy wing of overall $3^1A' \leftarrow X^1A_1$ electronic transition (of the Hartley band) is expected to decrease upon heavier oxygen substitution. (b) The intensity factors from X^1A_1 (0,0,0) to $3^1A'$ (ν_1,ν_2,ν_3) are (almost) systematically weaker for the heavier isotopologues than for the 666 isotopologue. This can be checked by comparing the intensity factors of 666 (Table 4 of the Supporting Information)[21] with those of the other isotopologues (Tables 5−9 of the Supporting Information).[21]

5. FRACTIONATION FACTORS IN THE HUGGINS RANGE

The ratio of "calculated" cross sections of two isotopologues (using the same ab initio PESs) is expected to be close to the experimental ratio. This expectation has been checked by comparing the ratio of the width of 888 and 666 experimental Hartley cross sections measured by Parisse et al.[32] with the same ratio for calculated cross sections.[12] These two pairs of cross sections have been fitted with the same analytic model and on the same energy range. The two width ratios, respectively, 1.0286 (exp) and 1.0298 (cal), are in good agreement. An additional check has been performed by comparing the calculated ratio of the 888 and 666 cross sections between 29 500 and 35 000 cm^{-1} with the corresponding experimental ratio obtained with the 666 and 888 cross sections recorded by Brion et al. These two ratios are shown in Figure 7. Above 35 000 cm^{-1} the two ratios are not shown because they are very close. The difference between the two ratios could be explained by the inaccuracy of the PESs but more likely by the uncertainty of the 888 experimental data (many works have been devoted to the 666 isotopologue). Moreover, the 888 and 666 recorded cross sections decrease by about 3 orders of magnitude from 35 000 cm^{-1} to 29 500 cm^{-1}. This may explain that the experimental cross section ratio is less accurate at 30 000 cm^{-1} than around 35 000 cm^{-1} and above

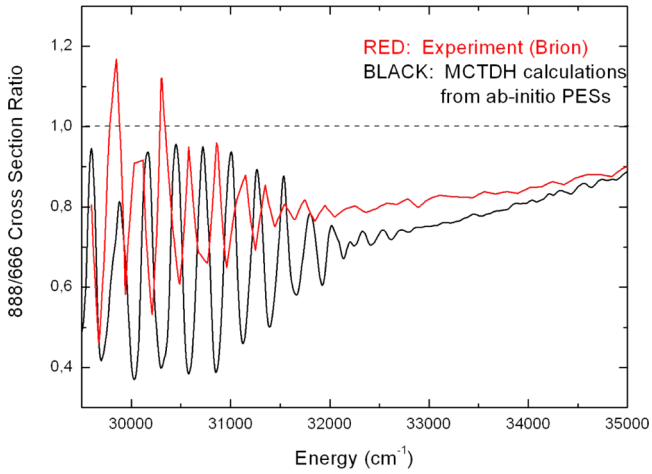

Figure 7. Calculated (black) and experimental (red) cross sections ratios of the $^{18}O_3$ (888) and the $^{16}O_3$ (666) isotopologues between 29 500 and 35 000 cm^{-1}. The experimental cross sections were recorded in similar conditions, and the calculated cross sections were smoothed in order to get a similar effective resolution. No shift was applied to the calculated data here. See text for discussion.

where the agreement is very satisfactory. The oscillations below 32 000 cm^{-1} are due to the shift of the "vibrational" structures between the 666 and the 888 isotopologues. These oscillations, which are expected to coincide, do not for two reasons: (a) the shift of 450 cm^{-1} discussed above is not applied here and (b) the ab initio and experimental frequencies of the "polyad structures" (about 250 cm^{-1}) are slightly different as discussed above. Globally, this comparison shows that the 888/666 calculated cross section ratio is in reasonable agreement with the corresponding experimental ratio, the observed differences being possibly due to an increasing experimental uncertainty at low energy. The calculated global cross sections (at 200 K) of the 667 and 676 isotopologues are shown with a log scale in Figure 8a and those of the 668 and 686 in Figure 8b. In both cases, the 666 calculated global cross section is plotted to allow a visual comparison. All the cross sections oscillate because of the polyad structures present for all the isotopologues. The polyads of the various isotopologues are almost "in phase" for the polyads $P = 0$ because their shifts are only due to the small ΔZPE (Figure 4). These shifts are negligible near 27 112 cm^{-1} (on the order of few inverse centimeters corresponding to the differences of the ΔZPE of the $3^1A'(0,0,0) \leftarrow X^1A_1(000)$ band origin of various isotopologues) and increase almost linearly with energy. At high energies, the polyads are broader and then smoother. Because of these shifts, the ratios of the cross section of each isotopologue with the one of the 666 isotopologue oscillate strongly in the Huggins range as it is shown in parts c and d of Figure 8. Similar oscillations have been obtained by Miller et al.[9] using the 888 and 666 experimental Huggins cross sections of Parisse et al.[32] Similarly, Danielache et al.[33] have found strong oscillations in their study of the isotopologues of SO_2 with various sulfur isotopes.

Ozone isotopologue enrichment due to ozone photolysis can be predicted from the energy (or wavelength) dependence of the fractionation factor of each isotopologue

$$\varepsilon_{abc}(E) = \{(\sigma_{abc}(E)/\sigma_{666}(E)) - 1\} \times 1000 \quad (7)$$

The fractionation factors are obtained from the ratios of cross sections. Ratios corresponding to the cross sections displayed in parts a and b of Figure 8 are plotted in Figure 9.

dx.doi.org/10.1021/jp3064382 | J. Phys. Chem. A 2012, 116, 12260−12270

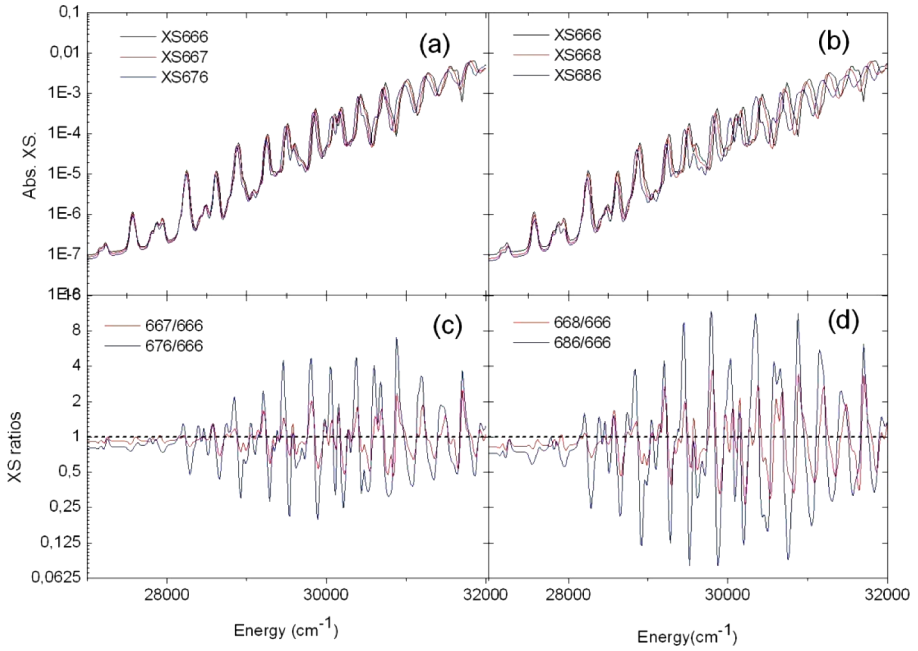

Figure 8. Calculated Huggins cross sections (log scale) vs photon energy for four isotopologues: (a) 667 and 676 isotopologues and (b) 668 and 686 isotopologues. The calculated cross section of the 666 isotopologue is shown for comparison. Parts c and d display the ratios (log scale) of these four isotopologue cross sections with the 666 cross section taken as a reference.

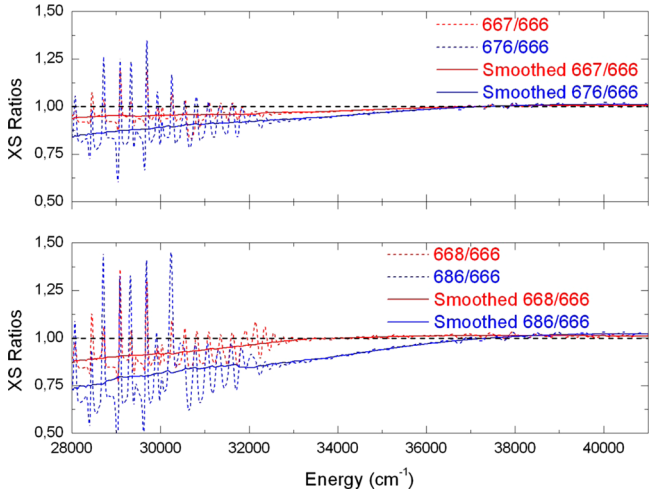

Figure 9. 667/666 and 676/666 cross section ratios (upper panel) and 668/666 and 686/666 cross section ratios (lower panel) vs photon energy are shown on the figure using a linear scale. The upper and lower panels, similar to parts c and d of Figure 7, respectively, are extended to the Hartley range up to 41 000 cm^{-1} and are obtained with two strong smoothing (over 300 and 3000 cm^{-1}, respectively) in order to reveal the global trends.

The oscillations of the cross section ratios (and then of the fractionation factors) are due to the shifts between polyad energies of the various isotopologues. These oscillations have been smoothed in order to get the energy dependence of the fractionation factor at a lower resolution which is more relevant for geophysical applications (e.g., when the cross sections are convoluted with the broad and rather smooth actinic flux in order to determine the photolysis rates).

Figure 9 shows the 667/666, 676/666, 668/666, and 686/666 σ ratios extended to the range 28 000−41 000 cm^{-1} including both the Huggins (Figures 6 and 8) band and the low-energy part of the Hartley band (Figure 7). Two different smoothing strengths have been chosen in order to show either the global trend or the superimposed oscillations due to the energy shift of the Huggins polyad patterns of the rare isotopologues compared to the one of 666. For example, the 668/666 ratio is the ratio of a 300 cm^{-1} smoothing of the 668 and 666 cross sections while the "smoothed 668/666" is a 3000-cm^{-1} smoothing of the 668/666 ratio. Figure 9 extends to low energies our previous results to the Huggins range which were obtained in the Hartley range (Figure 4 of paper I) only down to 32 000 cm^{-1} because of the numerical noise limitation mentioned above and present in Figure 5. Globally, the strong deviation from unity of these isotopologue cross section ratios observed on the low-energy range of the Hartley cross section is confirmed and reinforced in the Huggins range. The comparisons of cross section ratios obtained for the 667 and 668 isotopologues and for the 676 and 686 isotopologues show that the deviations from unity of these cross section ratios are mass dependent. These cross section ratios are expected to be almost independent of the temperature, except below ~29 000 cm^{-1} where the hot band contributions are significant. On the whole, a temperature increase is equivalent to a smoothing of the cross sections and of the cross section ratios. Note that similar but less accurate results have been previously obtained by Liang et al.[10] in the Hartley and the Chappuis ranges.

6. CONCLUSIONS AND PERSPECTIVES

We have determined the vibrational eigenstates (energy, wave function, assignment, and Franck−Condon factors) of the $3^1A'$ state for six ozone isotopologues, with special attention for the 866 and 766 asymmetric isotopologues, with quantum calculations using the MCDTH code. Note that experimental spectroscopic studies of isolated ozone isotopologues such as 866 or 686 are unlikely to be undertaken in near future because the synthesis of these isolated isotopologues is very difficult.[34] In contrast, quantum calculations using realistic PESs allow us

dx.doi.org/10.1021/jp3064382 | J. Phys. Chem. A 2012, 116, 12260−12270

to predict most of the isotopologue dependence of the spectroscopic properties of ozone.

All these eigenstates are organized in polyads because of the approximate 2:1:4 ratios between the three normal mode frequencies. Above ∼3000 cm^{-1} of vibrational energy (above the $3^1A'(0,0,0)$) a new family of eigenstates appears. This family, which is linked to a new periodic orbit extending along the dissociation coordinate, has been observed for each isotopologue.

By use of the vibrational energies and the Franck−Condon factors, we have determined the Huggins absorption cross sections of six isotopologues of ozone. These cross sections display a polyad structure vanishing progressively with increasing energy. The polyad structures of the various isotopologues are shifted from the ones of the 666 isotopologues. In the Huggins range, the smoothed cross sections of the various rare isotopologues of ozone are significantly smaller (up to 40% smaller for 686 isotopologue) than the one of the 666 isotopologue. This has a large impact on the atmospheric ozone photolysis rates because the solar flux is strongly screened mostly by the 666 isotopologue lying in the upper layers of the stratosphere: at altitudes below ∼35 km, the transmitted solar flux (which is able to dissociate the various ozone isotopologues) is mostly limited to the Chappuis and Huggins band because the strong Hartley band is completely "screened" by the ozone (mostly the 666 isotopologue) lying at higher altitude. Consequently, the photolysis rates of the rare and "heavy" isotopologues are significantly smaller than the one of the 666 isotopologue, leading to strong enrichments of these rare isotopologues. As a result of the screening effect of ozone on the solar flux, the ozone isotopologue enrichments due to the ozone photolysis by the sun are strongly dependent on the altitude. At high altitudes (above ∼50 km) the Hartley band plays a dominant role, and conversely, at low altitude, below ∼20 km, the Chappuis band becomes dominant. The isotope branching ratios calculated for the Hartley and Chappuis bands are very close to unity and then lead to weak enrichments in contrast with the Huggins band which induce much stronger enrichments and which play an important role between 20 and 50 km. This point has been partially put in evidence by Liang et al.,[10] but they have neglected the low-energy range of the Huggins band and consequently underestimate (up to a factor of 2) the enrichments due to the photolysis.

The atmospheric ozone isotopic enrichment results from both the destruction (by the photolysis process studied here and by the chemical reactions with NO_x, ClO_x, and HO_x[35]) and the formation processes (which favor the asymmetric isotopologues[4−6]). Note that the ozone formation process leads to mass-independent fractionation, while the photolysis process studied here is mass-dependent, and the mass dependences of the chemical reaction processes are unknown. Note also that the two destruction processes vary strongly with altitude and then play a different role in the stratosphere and in the troposphere. Chemical atmospheric models, like KINTECUS[36] or the one used by Liang et al.,[10] taking into account simultaneously all the isotope effects occurring in the ozone formation and the ozone destruction, seem to be able to predict the isotopic enrichments.[10] However, these chemical models require numerous reaction rates of which some are strongly dependent on the actinic flux and of the temperature and then of the altitude. With this goal in mind, the results presented in this paper for the 668 and 667 asymmetric isotopologues have been used to determine the dissociation branching ratio between the two dissociation isotopic channels,[37] respectively, 668 + $h\nu \Rightarrow$ 66 + 8 *or* 86 + 6 for 668 and 667 + $h\nu \Rightarrow$ 66 + 7 *or* 76 + 6 for 667. These branching ratios are expected to differ significantly from equality (fifty-fifty) in the Huggins range and then to significantly contribute to the overall atomic enrichments involving the 668 (and 667) isotopologue. This type of atomic oxygen enrichment occurs in addition to the isotopologue enrichment due the cross section ratios discussed in section 4 and will be presented in a forthcoming paper.[23]

■ ASSOCIATED CONTENT

Ⓢ Supporting Information

Tables of vibrational energies, assignments, and intensity factors of the four symmetric and the two asymmetric isotopologues and the Huggins cross sections of the 676, 686, 888, 667, and 668 isotopologues. This material is available free of charge via the Internet at http://pubs.acs.org.

■ AUTHOR INFORMATION

Corresponding Author

*E-mail: remy.jost@ujf-grenoble.fr. Phone: +33 4 76 51 43 34. Fax: +33 4 76 63 54 95.

Notes

The authors declare no competing financial interest.

■ ACKNOWLEDGMENTS

This work was supported by the ANR Project "IDEO" (NT09_436466). S.N. acknowledges financial support from the Agence Universitaire de la Francophonie (AUF). H.-D.M. acknowledges financial support by the Deutsche Forschungsgemeinschft (DFG).

■ REFERENCES

(1) Chapman, S.; Mem., R. *Meteorol. Soc.* **1930**, *3*, 103.
(2) Thiemens, M. H.; Heidenreich, J. E. *Science* **1983**, *219*, 1073.
(3) Mauersberger, K.; Morton, J.; Schueler, J.; Stehr, J.; Anderson, S. M. *Geophys. Res. Lett.* **1993**, *20*, 1031.
(4) Mauersberger, K.; Erbacher, B.; Krankowsky, D.; Günther, J.; Nickel, R. *Science* **1999**, *283*, 370.
(5) Gao, Y. Q.; Marcus, R. A. *Science* **2001**, *293*, 259.
(6) Hathorn, B. C.; Marcus, R. A. *J. Chem. Phys.* **1999**, *111*, 4087.
(7) Chakraborty, S. K.; Bhattacharya, J. *J. Chem. Phys.* **2003**, *118*, 2164.
(8) Cole, A. S.; Boering, K. A. *J. Chem. Phys.* **2006**, *125*, 184301.
(9) Miller, C. E.; Onorato, R. M.; Liang, M-C; Yung, Y. L. *Geophys. Res. Lett.* **2005**, *32*, L14814.
(10) Liang, M. C.; Irion, F. W.; Weibel, J. D.; Blake, G. A.; Miller, C. E.; Yung, Y. L. *J. Geophys. Res.* **2006**, *111*, D02302.
(11) Liang, M. C.; Blake, G. A.; Yung, Y. L. *J. Geophys. Res.* **2004**, *109*, D10308.
(12) Ndengué, S. A.; Gatti, F.; Schinke, R.; Meyer, H.-D.; Jost, R. *J. Phys. Chem. A* **2010**, *114*, 9855.
(13) Worth, G. A.; Beck, M. H.; Jäckle, A.; Meyer, H.-D. *The MCTDH Package*, version 8.2; University of Heidelberg: Germany, 2000. Meyer, H.-D. *The MCTDH Package*, Version 8.3 (2002), Version 8.4 (2007); University of Heidelberg: Germany. See http://mctdh.uni-hd.de.
(14) Meyer, H.-D.; Gatti, F.; Worth, G. A. *Multidimensional Quantum Dynamics: MCTDH Theory and Applications*; Wiley-VCH: Weinheim, 2009.
(15) Schinke, R.; McBane, G. C. *J. Chem. Phys.* **2010**, *132*, 044305.
(16) Meyer, H.-D.; Manthe, U.; Cederbaum, L. S. *Chem. Phys. Lett.* **1990**, *165*, 73.

(17) Beck, M. H.; Jäckle, A.; Worth, G. A.; Meyer, H.-D. *Phys. Rep.* **2000**, *324*, 1.
(18) Meyer, H.-D.; Le Quéré, F.; Léonard, C.; Gatti, F. *Chem. Phys.* **2006**, *329*, 179.
(19) Doriol, L. J.; Gatti, F.; Iung, C.; Meyer, H.-D. *J. Chem. Phys.* **2008**, *129*, 224109.
(20) Kosloff, R.; Tal-Ezer, H. *Chem. Phys. Lett.* **1986**, *127*, 223.
(21) Supporting Information.
(22) Grebenshchikov, S. Y.; Qu, Z.-W.; Zhu, H.; Schinke, R. *Phys. Chem. Chem. Phys.* **2007**, *9*, 2044.
(23) Ndengué, S. A.; Madronich, S.; Schinke, R.; Gatti, F.; Meyer, H.-D.; Jost, R. To be submitted to *J. Geophys. Res. D*.
(24) Qu, Z.-W.; Zhu, H.; Yu., S.; Grebenshchikov, R.; Schinke; Farantos, S. C. *J. Chem. Phys.* **2004**, *121*, 11731.
(25) Farantos, S. C.; Qu, Z.-W.; Zhu, H.; Schinke, R. *Int. J. Bifur. Chaos* **2006**, *16*, 1913.
(26) Katamaya, D. H. *J. Chem. Phys.* **1979**, *71*, 815.
(27) Joens, J. A. *J. Chem. Phys.* **1994**, *101*, 5431.
(28) O'Keeffe, P.; Ridley, T.; Lawley, K. P.; Donavan, R. J. *J. Chem. Phys.* **2001**, *115*, 9311.
(29) Note that in Figures 8 and 9 of ref 12, the polyad numbers are erroneous and should be shifted by one unit, e.g., $P = 5$ should be read as $P = 6$ and so on.
(30) Brion, J. Absorption cross section of $^{16}O_3$ at 218 K. High-resolution (0.01 nm) data obtained by personal communication from J. Brion, 1998.
(31) R. Schinke. *Photodissociation Dynamics*; Cambridge University Press: Cambridge, U.K., 1993.
(32) Parisse, C.; Brion, J.; Malicet, J. *Chem. Phys. Lett.* **1996**, *248*, 31.
(33) Danielache, S. O.; Eskebjerg, C.; Johnson, M. S.; Ueno, Y.; Yoshida, N. *J. Geophys. Res. Atmos* **2008**, *113*, D17314.
(34) Dimitrov, A.; Sepelt, K.; Scheffler, D.; Willner, H. *J. Am. Chem. Soc.* **1998**, *120*, 8711.
(35) *Scientific Assessment of Ozone Depletion: 2010, Global Ozone Research and Monitoring Project*; Report No. 52; World Meteorological Organization: Geneva, Switzerland, 2011.
(36) Ianni, J. C. *Kintecus*, Windows Version 2.80, 2002. www.kintecus.com.
(37) Ndengué, S. A.; Schinke, R.; Gatti, F.; Meyer, H.-D.; Jost, R. *J. Phys. Chem. A* **2010**, DOI: 10.1021/jp307195v.